Structural and Thermal Stabilities of Spinel LiMn$_2$O$_4$ Materials Under Commercial Power Batteries Cycling and Abusive Conditions

*Guo-Wei Ling[1], Xiping Zhu[2], Yan-Bing He[1, 3, *], Quan-Sheng Song[1], Baohua Li[3, *], Yong-Jin Li[1], Quan-Hong Yang[1,3], Zhi-Yuan Tang[1]*

[1] Department of Applied Chemistry, School of Chemical Engineering and Technology, Tianjin University, Tianjin 300072, China
[2] Ocell technology, Co., Ltd., Shenzhen, Guangdong 518109, China
[3] Key Laboratory of Thermal Management Engineering and Materials, Graduate School at Shenzhen, Tsinghua University, Shenzhen 518055, China
[*]E-mail: hezuzhang_2000@163.com , libh@mail.sz.tsinghua.edu.cn

The commercial 18650 spinel LiMn$_2$O$_4$/graphite high power batteries are prepared and the structural and thermal stabilities of the spinel LiMn$_2$O$_4$ cathode materials under high rate cycling and abusive conditions are investigated using the commercial 18650 LiMn$_2$O$_4$/graphite high power batteries. Results show that the batteries present the best power performance when the compaction density of LiMn$_2$O$_4$ electrode is 2.93g cm^{-3}. The microstructure of LiMn$_2$O$_4$ materials undergoes obvious distortion due to the Mn dissolution after the LiMn$_2$O$_4$ power batteries have been subjected to 100 cycles with discharge rate of 8 C at 25 $^{\circ}$C and discharge rate of 5C at 55 $^{\circ}$C. The charge-transfer resistance (R_{ct}) of power batteries after cycling at high temperature rises significantly. During battery overcharge, the solid electrolyte interface (R_{sei}) and R_{ct} of power batteries increase greatly and the electrolyte shows obviously less reaction activities on LiMn$_2$O$_4$ electrode than on Li(Ni$_{1/3}$Co$_{1/3}$Mn$_{1/3}$)O$_2$ electrode. The reactions of fully charged LiMn$_2$O$_4$ cathodes and graphite anodes with electrolyte inside battery during battery overcharge and oven tests can be activated at much lower temperature than that outside battery, while these reactions do not occur during short current test in the fully charged batteries.

1. INTRODUCTION

The spinel LiMn$_2$O$_4$ is one of the most promising alternative cathode materials for lithium-ion power batteries, which is due to the advantages such as low cost, good environmental compatibility,

and good thermal stability. MacNeil et al [1]. reported that the charged $LiMn_2O_4$ material shows obviously higher thermal stability in the electrolyte at high temperature than $LiCoO_2$ and $LiNiO_2$. The good thermal stability of spinel $LiMn_2O_4$ is beneficial for its use in high power batteries [2]. However, the spinel $LiMn_2O_4$ materials show significant capacity fading during storage and cycling at room and high temperatures due to the Mn dissolution into the electrolyte and $LiMn_2O_4$ suffering from large Jahn-Teller (J-T) instability caused by Mn^{3+} at the octahedral sites [3-9]. At present, the researchers have taken effective measures to improve the electrochemical and high temperature performance of $LiMn_2O_4$ including metal ions doping, metal oxide coating and reducing the particle size of $LiMn_2O_4$[10-17].

So far, the electrochemical performance of $LiMn_2O_4$ materials has been mainly investigated using coin cells, and their thermal stability has been mainly analyzed by examining the reactivity of $LiMn_2O_4$ materials with electrolyte at high temperatures using differential scanning calorimetry (DSC) and C80 calorimeter [1,18]. It has been found that the mainly exothermic reactions between fully or overcharged $LiMn_2O_4$ and electrolyte outside battery occur at around 250 ^oC. In fact, from our previous report [19], we have found the reaction temperature of $Li(Ni_{1/3}Co_{1/3}Mn_{1/3})O_2$ materials with electrolyte, which occurs inside batteries, is much lower than that outside batteries. The electrolyte shows much higher thermal reaction activity on the fully charged $Li(Ni_{1/3}Co_{1/3}Mn_{1/3})O_2$ electrode inside batteries than outside batteries. However, until now, we do not know the thermal reactivity of electrolyte on the $LiMn_2O_4$ electrode under abusive conditions of commercial power batteries. Thus, it is very significant to investigate the structural and thermal stabilities of $LiMn_2O_4$ materials inside the power batteries.

In this work, we prepared the commercial 18650 $LiMn_2O_4$/graphite high power batteries and investigated the effects of compaction density on the rate discharge performance high power batteries. And then we further investigated the structural and thermal stability of $LiMn_2O_4$ cathode materials under high rate cycling at 25 and 55 ^oC and abusive conditions in 18650 $LiMn_2O_4$/graphite high power batteries and revealed the heating mechanism of the high power batteries.

2. EXPERIMENTAL

2.1 Preparation of power batteries

18650 $LiMn_2O_4$/graphite high power batteries were assembled (18 mm in diameter and 65 mm in height). The nominal capacity of the batteries was designed to be 1200 mAh. The batteries used spinel $LiMn_2O_4$ (Hunan Rui Xiang Science and Technology Co., Ltd, China) as the cathode material, graphite as the anode material, and polyethylene as a separator. The $LiMn_2O_4$ cathodes consisted of 90 wt% spinel $LiMn_2O_4$, 5 wt% conductive carbon black(Super-P), and 5 wt% poly(vinylidene fluoride) (PVDF). The graphite anodes consisted of 93 wt% composite graphite, 2.5 wt% styrene-butadiene rubber (SBR), 1.5 wt% carboxymethyl cellulose (CMC) and 3 wt% Super-P. 1 M $LiPF_6$ in a 1:1:1 mixture of ethylene carbonate(EC), dimethyl carbonate(DMC) and ethylene methyl carbonate(EMC) (1 M $LiPF_6$/ EC+DMC+EMC) was used as the electrolyte. Positive electrodes were made by coating

the mixing slurry of $LiMn_2O_4$ active material, conductive carbon black, and PVDF on an aluminum foil collector. The loading amount of the cathode materials on each side of the electrodes was about 15 mg cm^{-2}. The cathode sheets were compressed to different thickness and make the cathodes have different compaction density. Negative electrodes were prepared by coating the mixing slurry of composite graphite, SBR, CMC and Super-P on a copper foil. The loading amount of the anode materials on each side of the electrodes was about 5.5 mg cm^{-2}. The thickness of the anode electrode was about 85 μm. The injection of the electrolyte was conducted in an argon filled glove box.

2.2 Characterization of power batteries

The formation, rate-discharge performance, capacity and cycling performance tests of the batteries were performed by using the BS-9300 and BS-9366 lithium-ion battery testers. Since the most recent industrial formation process includes only one cycle, the experimental batteries in this work also underwent one cycle of charge-discharge for the formation. After the formation, all batteries were charged and discharged three times between 2.75 and 4.20 V at a current of 600 mA (0.5 C), which could stabilize the performance of the batteries. The cycling performance of the batteries was examined between 2.75 and 4.20 V. The batteries were charged with a current of 600 mA (0.5 C) and discharged with different currents during cycling at 25 and 55 ^{o}C.

The electrochemical working station (Gamry Instrument model PCI 4-750) was used to measure the EIS of the 18650 $LiMn_2O_4$/graphite power batteries. The EIS of the batteries before and after cycling with 50% states of charge (SOC) were measured at the open circuit voltage (OCV) of the batteries with $LiMn_2O_4$ cathode as the working electrode and graphite anode as counter electrode. The impedance was measured by applying a 5 mV of ac oscillation with the frequency ranging from 100 kHz to 0.01 Hz.

2.3 Structure characterization of $LiMn_2O_4$ materials before and after cycling

The fully discharged high power batteries before and after cycling were transferred to a glove box and then dissembled. The $LiMn_2O_4$ cathode was rinsed using dimethyl carbonate (DMC) to remove the electrolyte from the cathode surface. Then, the $LiMn_2O_4$ samples were taken from the cathode and dried in the glove box antechamber to remove the residual DMC. X-ray diffraction (XRD) patterns of the $LiMn_2O_4$ samples before and after cycling were obtained by a PANAlytical X'Pert powder diffractometer using Co Kα radiation in an angular range of 10-90° (2θ) with a 0.02^{o} (2θ) step.

2.4 Abusive tests of power batteries

The overcharge tests were conducted by further charging the batteries with a constant current of 1.2 A (1 C) using a 10 V power supply (1 C/10 V) after they were fully charged to 4.2 V. The oven tests were conducted in the way that the batteries were fully charged to 4.2 V and then laid in an oven, and the oven temperature was then raised from environment temperature and kept stable at 150 ^{o}C. The

short current tests were conducted by connecting the cathode tab with the anode tab using a low resistance lead (<5 mΩ) after the batteries were fully charged to 4.2 V. A multimeter was also connected to the cathode and anode tab to measure the battery voltage in the short circuit experiment. A type-K thermal couple was attached to the surface of batteries to record the temperature change during the abusive tests. The EIS of batteries before (4.2 V) and after the overcharge (4.8 and 5.0 V) tests were measured.

3. RESULTS AND DISCUSION

### 3.1 Structural stability of LiMn$_2$O$_4$ materials during cycling

(a)

(b)
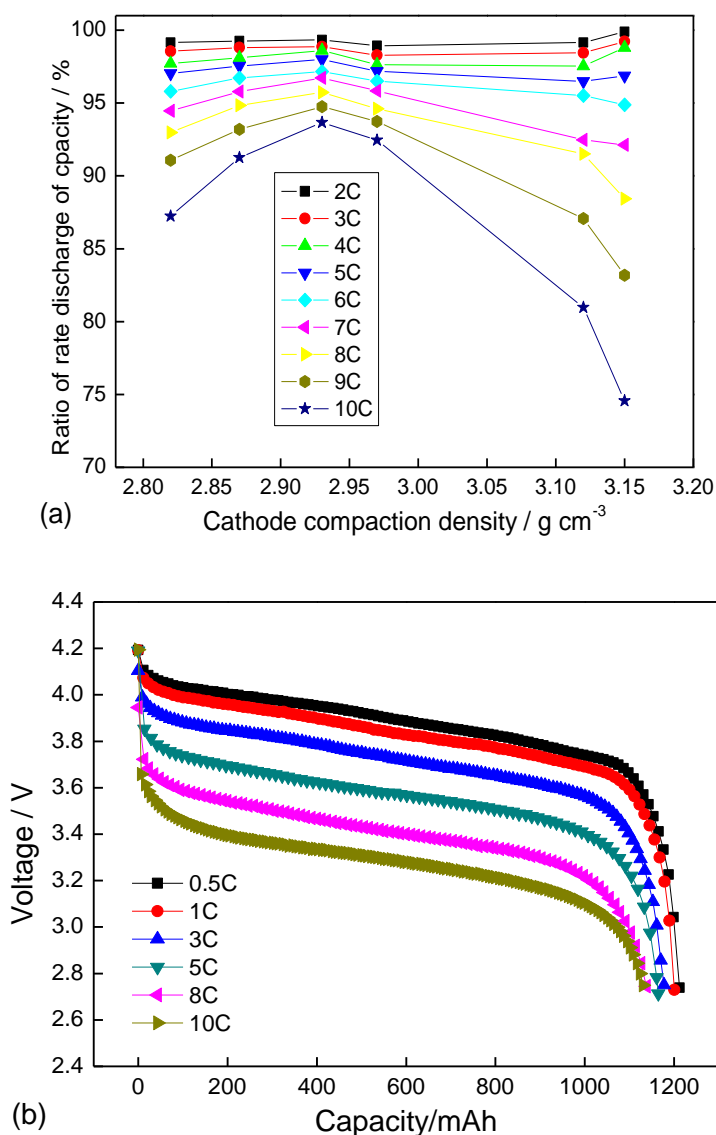
Figure 1. Relationship between rate discharge performance and compaction density of spinel LiMn$_2$O$_4$ electrode in 18650 LiMn$_2$O$_4$/graphite high power batteries (a); rate discharge performance of 18650 spinel LiMn$_2$O$_4$/graphite power batteries at 25 ^{o}C (b).

The effects of compaction density on the performance of $LiMn_2O_4$ electrode were investigated and the aim is to assemble the best power performance 18650 $LiMn_2O_4$/graphite batteries. It can be seen from Fig.1a that the batteries show quite different rate discharge performance when the $LiMn_2O_4$ electrodes are under different compaction density, and the rate discharge performance is best when the compaction density of $LiMn_2O_4$ electrode is 2.93 g cm^{-3}. Its discharge capacity at rates of 5, 8 and 10 C is respective 97.99%, 95.73% and 93.67% of that at 1 C rate. These results show that the power batteries can be discharged at a high current to deliver most of their capacity, indicating good kinetic characteristics for the power batteries. However, it can be seen from Fig. 1b that the discharge voltage is distinctly reduced with the increase in discharge rate. This may be attributed to the large polarization at a high discharge current and the relatively slow lithium-ion diffusion rate in solid phase and electrolyte.
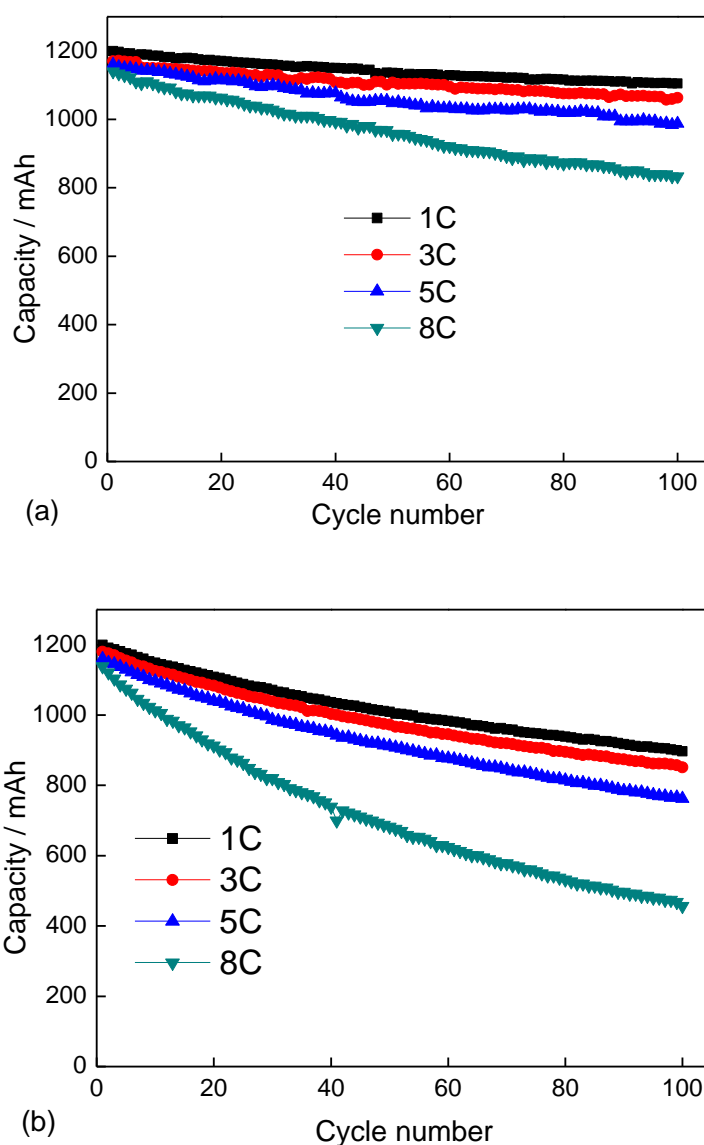

Figure 2. Cycling performance of 18650 spinel $LiMn_2O_4$/graphite power batteries with various discharge rates at 25 ^{o}C (a) and 55 ^{o}C (b).

Structural stability of LiMn$_2$O$_4$ materials during cycling at 25 and 55 ^{o}C was investigated by cycling the 18650 LiMn$_2$O$_4$/graphite high power batteries for up to 100 times with different discharge rates. It can be obtained from Fig. 2a that the capacity retention for the discharge rates of 1, 3, 5 and 8 C after 100 cycles at 25 ^{o}C are 92.10, 90.86, 85.18 and 73.07%, respectively. This indicates that the capacity loss increases with the increase in the discharge rate during cycling. The battery temperature increases gradually during high rate discharge, which not only accelerates the Mn dissolution, but also results in more consumption of electrolyte [5,8,20]. Thus, the capacity loss is larger at high-rate discharge during cycling. When the power batteries are cycled with various discharge rates at 55 ^{o}C, it can be obtained from Fig. 2b that the capacity retention rate for the discharge rates of 1, 3, 5 and 8 C after 100 cycles are 74.72, 72.17, 65.70 and 40.11%, respectively. It is obvious that the capacity loss increases with the increase in the discharge rate, especially for the discharge rate of 8 C. In addition, it also can be found that the batteries show obviously worse performance at 55 ^{o}C than that at 25 ^{o}C.
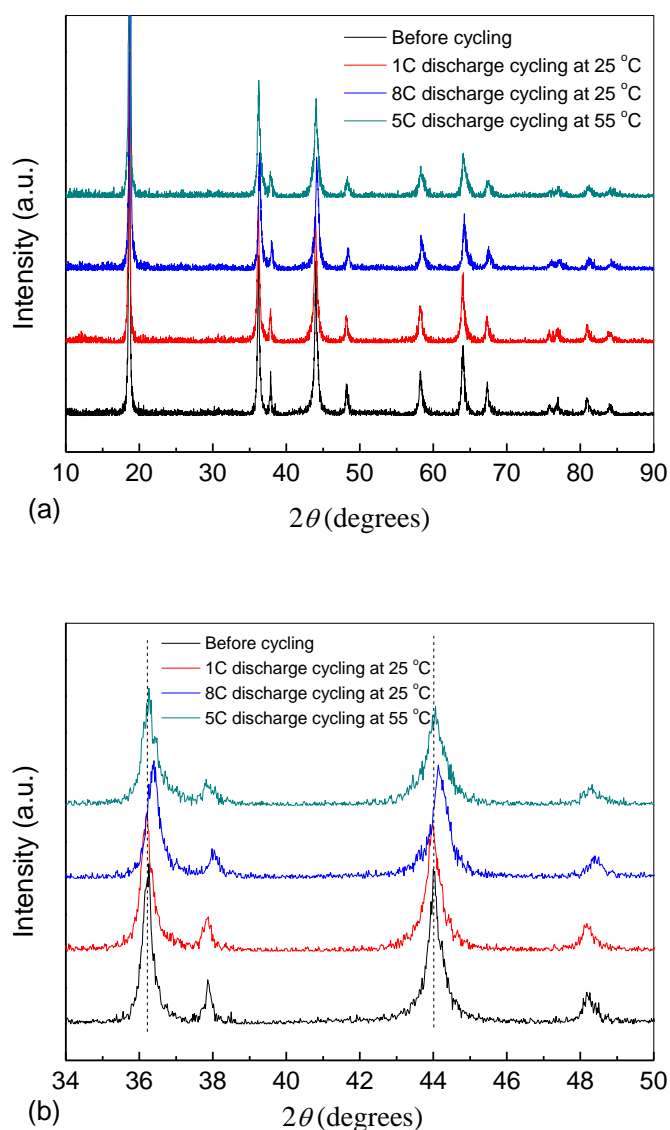
Figure 3. XRD patterns of LiMn$_2$O$_4$ materials before and after 100 cycles at 25 ^{o}C and 55 ^{o}C within the 2θ angles range of 10~90° (a) and 34~50^o(b).

　　　　XRD patterns of fully discharged spinel LiMn₂O₄ materials before and after cycling are shown in Fig. 3. It can be seen that the LiMn₂O₄ materials maintain their spinel structure even having been subjected to 100 cycles with discharge rate of 8 C at 25 °C and discharge rate of 5C at 55 °C. However, the XRD peaks of the LiMn₂O₄ after cycling become wider and lower as compared with those of the material before cycling, especially for the LiMn₂O₄ cycled at 55 °C, which suggests that the microstructure of LiMn₂O₄ undergoes obvious distortion and leads to the relatively poor cycling performance of power batteries at high charge/discharge rates and working temperature.
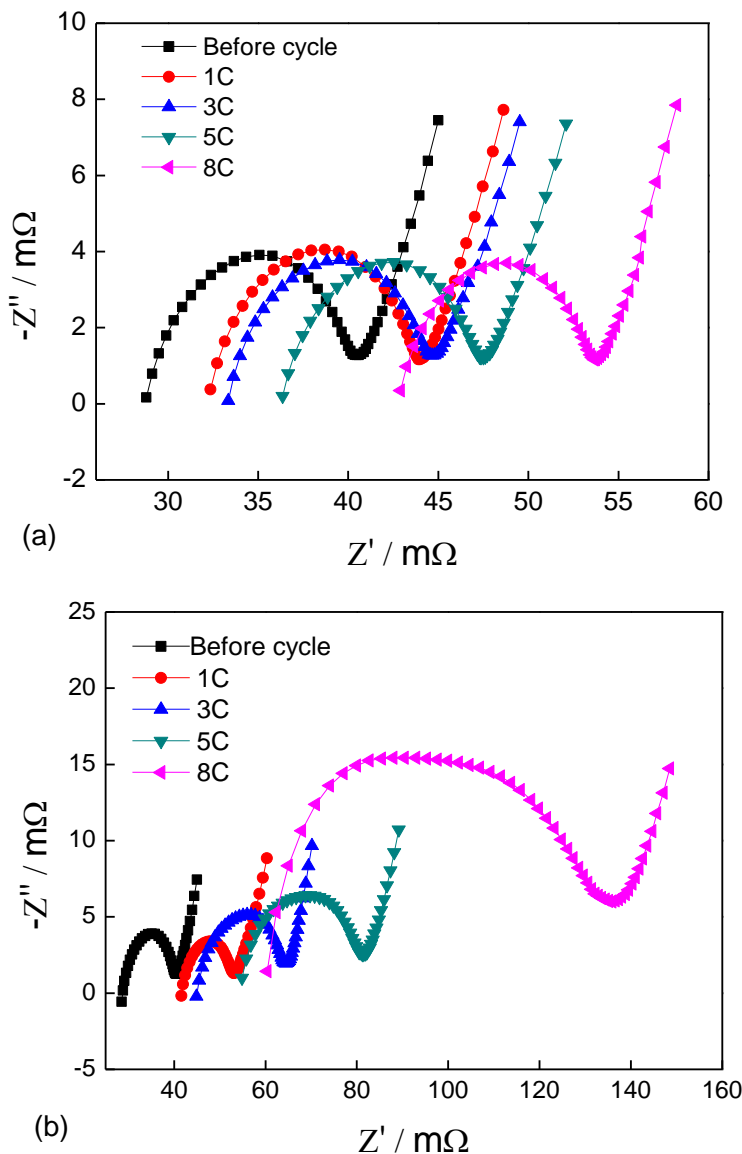
Figure 4. EIS of 18650 spinel LiMn₂O₄/graphite power batteries with 50% SOC, which were cycled 100 times with various discharge rates at 25 °C (a) and 55 °C (b).

　　　　The EIS of 18650 spinel LiMn₂O₄/graphite power batteries at half charge state after 100 cycles at 25 and 55 °C with various discharge rates are plotted in Fig. 4. It can be seen that the EIS consists of one depressed semicircle at high to medium frequency and a straight line at low frequency. The
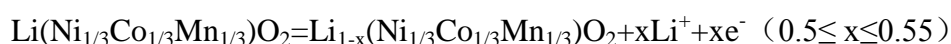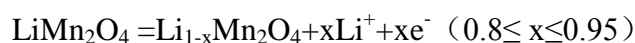
intersection of the diagram with the real axis refers to a bulk resistance (R_b), which mainly reflects the sum of ohmic resistances of the electrolyte, separator and electrodes. The depressed semicircle at high to medium frequency corresponds to the charge-transfer resistance (R_{ct}) and CPE. CPE are the constant phase elements, which were used instead of double-layer capacitance (C_{dl}). Warburg impedance at low frequency is related to the diffusion of Li ions on the interface between the active material particles and the electrolyte [21-23]. The value of the resistance of the solid electrolyte interface (R_{sei}) formed on the surface of two electrodes may be very little, thus, the semicircle at high frequency which represents R_{sei} is covered by the semicircle of charge-transfer resistance.

It can be seen from Fig. 4a that the R_b of all batteries increases after 100 cycles at 25 °C, while the R_{ct} has not obvious change. The increase in R_b with cycle number is attributed to the related consumption of electrolyte [22]. Fig. 4b indicates that the R_b increases with the increase in the discharge rate, and the increase is much greater when the discharge rate increases from 5 to 8 C. The R_{ct} almost does not change after 100 cycles at the discharge rate of 1 C, while it increases gradually from 3 to 5 C, and increases significantly from 5 to 8 C. The battery temperature can reach 80 °C at the end of discharge with discharge rate of 8 C in the environment of 55 °C. Thus, the Mn dissolution and the electrolyte decomposition are accelerated greatly [6], which result in the significant increase of the R_b and R_{ct}. It can be further confirmed that the microstructure of the spinel $LiMn_2O_4$ cathode is distorted greatly after 100 cycles at 55 °C with the discharge rate of 5 and 8 C.

### 3.2. Thermal stability of spinel LiMn₂O₄ materials under abusive conditions

18650 $LiMn_2O_4$/graphite high power batteries were overcharged by 1 C/10 V to investigate the thermal stability and reveal the heating mechanism of the batteries. It can be observed from Fig. 5a that the $LiMn_2O_4$/graphite high power batteries shows obviously different overcharge characteristics with those of $Li(Ni_{1/3}Co_{1/3}Mn_{1/3})O_2$/graphite high power batteries as shown in our previous work [19]. After the $LiMn_2O_4$ batteries have been overcharged for only about 6 min, the battery voltage can reach 4.8 V, while this process needs about 30 min for $Li(Ni_{1/3}Co_{1/3}Mn_{1/3})O_2$ batteries.

It is well-known that the electrochemical reaction for the spinel $LiMn_2O_4$ and $Li(Ni_{1/3}Co_{1/3}Mn_{1/3})O_2$ electrode during charge are as follows, respectively:

$$LiMn_2O_4 = Li_{1-x}Mn_2O_4 + xLi^+ + xe^- \quad (0.8 \leq x \leq 0.95)$$

$$Li(Ni_{1/3}Co_{1/3}Mn_{1/3})O_2 = Li_{1-x}(Ni_{1/3}Co_{1/3}Mn_{1/3})O_2 + xLi^+ + xe^- \quad (0.5 \leq x \leq 0.55)$$

It can be found that the number of deintercalated Li ions is quite different when these two types materials are fully charged. After the $LiMn_2O_4$ electrode is fully charged, above 80% Li ions are deintercalated from $LiMn_2O_4$. However, for the fully charged $Li(Ni_{1/3}Co_{1/3}Mn_{1/3})O_2$, only less than 55% Li ions are pulled out from the $Li(Ni_{1/3}Co_{1/3}Mn_{1/3})O_2$. Thus, when the fully charged $LiMn_2O_4$ is overcharged, there are few Li ions that can be deintercalated from $LiMn_2O_4$, which leads to the quick increase of battery voltage during overcharge. Nevertheless, the Li ion concentration in the fully

charged $Li(Ni_{1/3}Co_{1/3}Mn_{1/3})O_2$ is still close to 45%, and this means that there are enough Li ions that can be deintercalated from fully charged $Li(Ni_{1/3}Co_{1/3}Mn_{1/3})O_2$ under overcharge condition. Therefore, the voltage of $Li(Ni_{1/3}Co_{1/3}Mn_{1/3})O_2$ batteries does not increase quickly during overcharge.
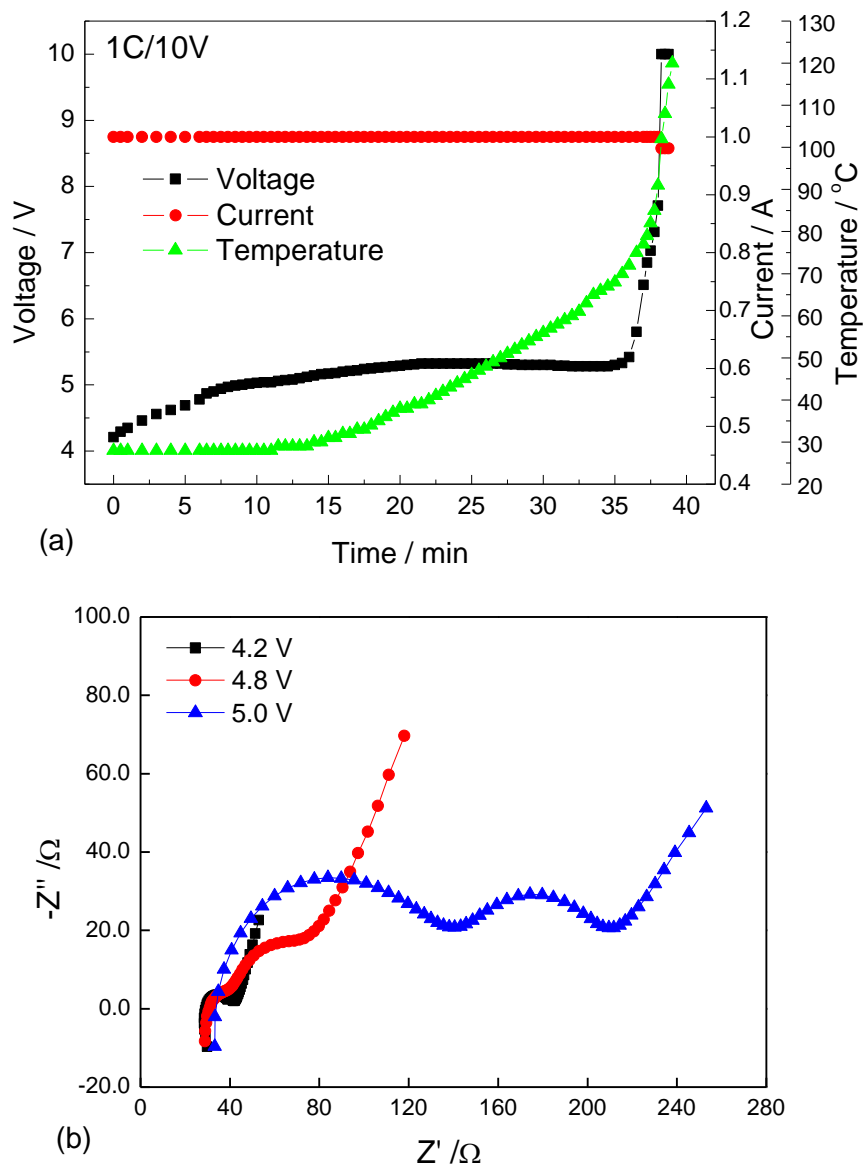
Figure 5. Voltage, current and temperature curves of 18650 $LiMn_2O_4$/graphite high power batteries during 1 C/10 V overcharge test (a); EIS of power batteries before (4.2 V) and after overcharge(4.8 and 5.0 V) (b).

It also can be seen that the battery voltage increases gradually during the overcharge. The battery temperature starts to increase when the batteries are overcharged to 5.0 V and goes up quickly from 5.15 V. Thus, within the voltage range of 5.0~5.15 V, the exothermic reactions, such as the electrolyte decomposition, the reaction between the delithiated cathode and the electrolyte, and the violent reaction between the overcharged anode and the electrolyte do not occur.

The EIS of high power batteries at 4.2 (before overcharge) and 4.8 and 5.0 V (after overcharge) are plotted in Fig. 5b. It can be seen that the total resistance R_{cell}, which is composed of R_b, R_{sei} and R_{ct}, increases greatly after overcharge due to the significant increase in R_{sei} and R_{ct}. Fig. 5a shows that the battery voltage increases from 4.2 to 5.0 V after the batteries are overcharged for about 6 min. At this stage, the delithiation of overcharged $LiMn_2O_4$ materials becomes very difficult due to a much lower lithium ion concentration in the overcharged $LiMn_2O_4$ materials, which results in the great increase in the electrochemical reaction resistance as shown in Fig. 5b. In addition, the lithium ions cannot be inserted into the fully lithiated graphite anode and they will be deposited on the surface of graphite anode to form lithium metal, which leads to the great increase of R_{sei}. The increase of R_{cell} makes the batteries generate some Joule heat during overcharge. If the heat generation and dissipation are in balance, the battery temperature will not change. This occurs only when the batteries are overcharged to below 5.0 V. When the batteries are overcharged to above 5.0 V and the rate of heat generation is higher than that of heat dissipation, this balance will be broken and the battery temperature will rise. Thus, the increase in the battery temperature during overcharge from 5.0 to 5.15 V is attributed to the Joule heat, which is generated from the great increase of R_{cell}.

The battery temperature goes up quickly after the battery is overcharged to 5.15 V. It also can be seen that the voltage shows some complicated changes from 5.15 V, where it increases slowly from 5.15 to 5.32 V and subsequently shows a short plateau for about 6 min, then decreases gradually to 5.28 V and increases rapidly again. The voltage change starting above 5.15 V is a typical symbol of electrolyte decomposition on the $LiMn_2O_4$ electrode. In our previous work[19], we have known that the electrolyte is first oxidized on the overcharged $Li(Ni_{1/3}Co_{1/3}Mn_{1/3})O_2$ cathode when the batteries are overcharged to 4.90 V, and the reaction between the electrolyte and overcharged cathode generates much gases and heat, which leads to a great increase of battery temperature. Thus, the electrolyte shows obviously less reaction activities on the $LiMn_2O_4$ electrode than on the $Li(Ni_{1/3}Co_{1/3}Mn_{1/3})O_2$ electrode.

When the battery voltage reaches 5.32 V, the voltage of the overcharged batteries shows a short plateau at the overcharging time of 21-27 min. This may be because the amount of the charge consumed by the reaction of the electrolyte and overcharged cathode is equal to that supplied by the overcharge. The exothermic reaction rate of the overcharged cathode and electrolyte will increase along with the rise of the battery temperature. In this period, the temperature increases quickly, which is attributed to that most of the applied electric energies are converted to heat. When the charge consumption exceeds the charge supply from overcharge, and the anode and cathode materials are destroyed severely due to the reaction of electrodes with electrolyte, which causes the gradual decrease in battery voltage. The quantity of the electrolyte gradually decreases with the electrolyte decomposition. The amount of the charge consumed by the electrolyte decomposition is less than that supplied by the overcharge, which leads to the rise of the battery voltage again. It can be observed that the battery temperature increase rapidly from at around 80 $^{\circ}$C. This suggests that the reactions of overcharged graphite anode (with deposited lithium metal) and the electrolyte solvents are activated by the thermal and electric potential energies, which generates much gases and heat that contributes to a rapid increase of battery temperature.

Short current of power battery also was tested as shown in Fig. 6a. It can be seen that the voltage decreases to about 0.7 V and subsequently shows a short plateau, and then rapidly decreases to 0 V. The battery temperature rises greatly to the maximum value of about 118 °C. The batteries are heated much rapidly by the irreversible heat generation from the current passing through the electrodes. It can be seen that the batteries are not runaway and the battery temperature starts to decrease at the end of discharge plateau. Thus, the reactions of the $LiMn_2O_4$ cathode and graphite anode with the electrolyte cannot be activated during the short current test of the batteries.
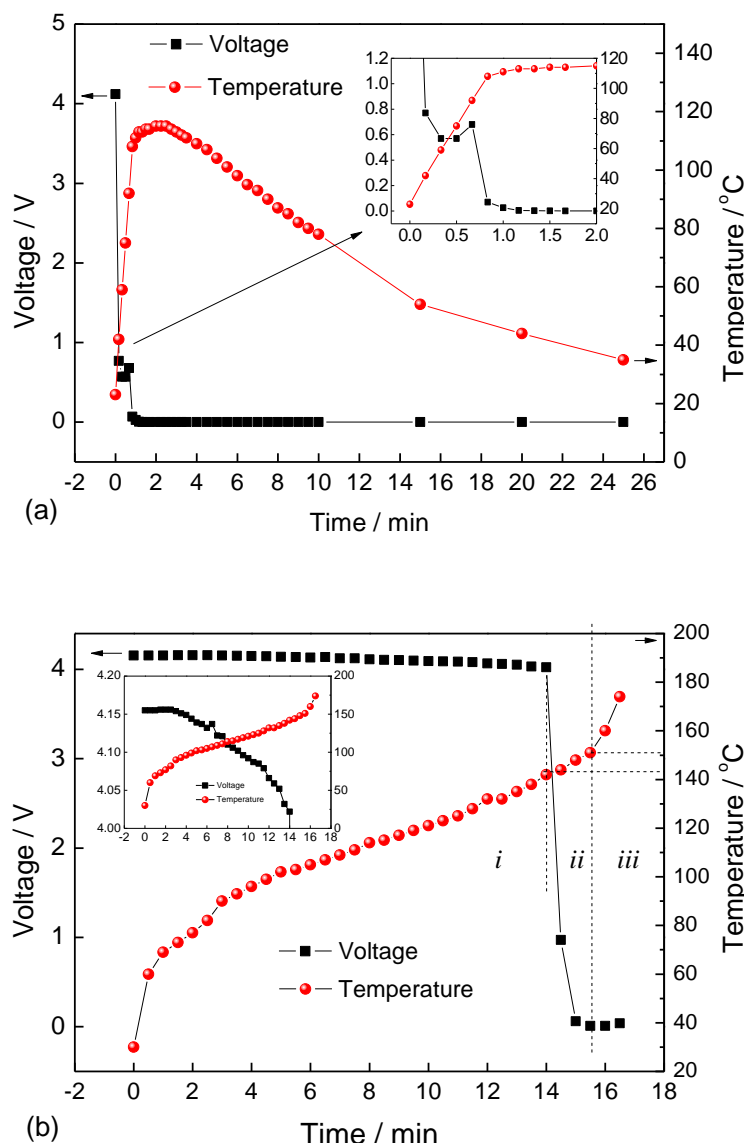
Figure 6. Voltage and temperature curves of fully charged 18650 $LiMn_2O_4$/graphite high power batteries during short current (a) and oven test at 150 ^{o}C (b).

When the battery was subjected to the oven test, it can be observed from Fig. 6b that the battery voltage and temperature changes mainly include three stages (*i, ii* and *iii*). At the first stage (*i*), the battery temperature increases gradually with the oven temperature and the voltage of fully charged

batteries decreases when the battery temperature increases to about 90 ^{o}C, especially from 129 ^{o}C. This indicates that the self-discharge of batteries becomes serious at high temperature and the decomposition of SEI film occurs from 129 ^{o}C. In this stage, the violent chemical reactions do not occur inside battery. At the second stage (*ii*), the battery voltage decreases rapidly from around 141 ^{o}C, and in this stage, the battery temperature increase quickly to about 150 ^{o}C. The separator of polyethylene membrane may shrink when the battery temperature is higher than 140 ^{o}C, which may lead to physical contact of cathode and anode that result in circuit shorting of battery. Fig. 6a has shown that the battery voltage decreases rapidly to about 0 V within one minute when the battery is under fully short current. Thus, it can be concluded that the fully short current of battery occur during oven test due to the separator shrinkage or partial/local melting. The heat resulting in from the circuit shorting makes the battery temperature increase quickly. At the third stage (*iii*), the battery temperature rises rapidly to 174 ^{o}C and the battery explodes. This suggests that the reactions of the lithiated graphite anode and delithiated $LiMn_2O_4$ cathode with the electrolyte take place at around 150 ^{o}C in the fully charged batteries, which make the battery temperature exceed 150 ^{o}C. Thus, the reactivity of the delithiated $LiMn_2O_4$ cathode and lithiated graphite anode with the electrolyte inside battery is very different with that outside battery. The temperature required for the reactions inside batteries of about 150 ^{o}C is much lower than the temperature of about 250 ^{o}C required for the reactions outside batteries. These reactions are activated by thermal and electric potential energies together.

3. CONCLUSIONS

In this work, the 18650 spinel $LiMn_2O_4$/graphite high power batteries were subjected to 100 cycles with charge rate of 0.5C and discharge rate of 1, 3, 5 and 8 C at 25 and 55 ^{o}C, respectively. It has been found that $LiMn_2O_4$ materials maintain their spinel structure, whereas their microstructure has obvious distortion, which leads to the relatively poor cycling performance of power batteries at high discharge rates and working temperature. During 1C/10V overcharge, the $LiMn_2O_4$/graphite high power batteries show significantly different overcharge characteristics with those of $Li(Ni_{1/3}Co_{1/3}Mn_{1/3})O_2$/graphite high power batteries. The $LiMn_2O_4$ /graphite batteries, which are overcharged to 4.8 V, need only for about 6 min, while this process needs about 30 min for $Li(Ni_{1/3}Co_{1/3}Mn_{1/3})O_2$ /graphite batteries. The electrolyte is oxidized on the $LiMn_2O_4$ electrode when the battery voltage increases to 5.15 V and the total resistance (R_{cell}) of battery increases significantly, which lead to the quick increase in the battery temperature. The reactions inside the battery during overcharge can be activated by the thermal and electric potential energies cooperatively, which make the reactions of graphite anode with the electrolyte occur only at around 80 ^{o}C. These reactions also can be activated at about 150 ^{o}C inside fully charged battery during oven test, which is much lower than the temperature of about 250 ^{o}C required for the reactions outside battery.

SG200810150054A), Guangdong Province Innovation R&D Team Plan for Energy and Environmental Materials.

References

1. D. D. MacNeil, Z. Lu, Z. Chen, J. R. Dahn, *J. Power Sources* 108 (2002) 8.
2. P. Baurlein, R. Herr, M. Kloss, J. Kumpers, M. Maul, E. Meissner, *J. Power Sources* 82 (1999) 585.
3. M. Wohlfahrt-Mehrens, C. Vogler, J. Garche, *J. Power Sources* 127 (2004) 58.
4. Y. Shiraishi, I. Nakai, T. Tsubata, T. Himeda, F. Nishikawa, *J. Power Sources* 81-82 (1999) 571.
5. T. Aoshima, K. Okahara, C. Kiyohara, K. Shizuka, *J. Power Sources* 97-98 (2001) 377.
6. X. Wang, Y. Yagi, Y.-S. Lee, M. Yoshio, Y. Xia, T. Sakai, *J. Power Sources* 97-98 (2001) 427.
7. M.-K. Kim, H.-T. Chung, W.-S. Um, Y.-J. Park, J.-G. Kim, H.-G. Kim, *Mater. Lett*. 39 (1999.) 133.
8. A. d. Pasquier, A. Blyr, A. Cressent, C. Lenain, G. Amatucci, J. M. Tarascon, *J. Power Sources* 81-82 (1999) 54.
9. A. Yamada, M. Tanaka, K. Tanaka, K. Sekai, *J. Power Sources* 81-82 (1999) 73.
10. D. Capsoni, M. Bini, G. Chiodelli, P. Mustarelli, V. Massarotti, C. B. Azzoni, M. C. Mozzati, L. Linati, *J. Phys. Chem*. B 106 (2002,) 7432.
11. D. Capsoni, M. Bini, G. Chiodelli, V. Massarotti, P. Mustarelli, L. Linati, M. C. Mozzati, C. B. Azzoni, *Solid State Commun*. 126 (2003) 169.
12. H.-W. Ha, N. J. Yun, K. Kim, *Electrochim. Acta* 52 (2007) 3236.
13. G. S. Chen, G. S. Chen, H. H. Hsiao, R. F. Louh, C. J. Humphreysc, *Electrochem Solid* St 7 (2004) A235.
14. K.Suryakala, G. P. Kalaignan, T.Vasudevan, *Int. J. Electrochem. Sci*. 1 (2006) 372.
15. L. Wang, J. Zhao, S. Guo, X. He, C. Jiang, C. Wan, *Int. J. Electrochem. Sci*. 5 (2010) 1113.
16. K.Suryakala, KR.Marikkannu, G. P. Kalaignan, T.Vasudevan, *Int. J. Electrochem. Sci*. 3 (2008) 136
17. M. A. Kiani, M. F. Mousavi, M. S. Rahmanifar, *Int. J. Electrochem. Sci*. 6 (2011) 2581.
18. Q. S. Wang, J. H. Sun, C. H. Chen, *J. Electrochem. Soc*. 154 (2007) A263.
19. Y.-B. He, F. Ning, Q.-H. Yang, Q.-S. Song, B. Li, F. Su, H. Du, Z.-Y. Tang, F. Kang, *J. Power Sources* 196 (2011) 10322.
20. A. M. Andersson, K. Edstrom, N. Raob, A.Wendsjo, *J. Power Sources* 81-82 (1999) 286.
21. S. S. Zhang, K. Xu, T. R. Jow, *J. Power Sources* 160 (2006) 1403.
22. S. S. Zhang, *J. Power Sources* 161 (2006) 1385.
23. S. S. Zhang, K. Xu, T. R. Jow, *Electrochim. Acta* 49 (2004) 1057